# Ultralow Noise Optical Frequency Combs

Mamoru Endo , Tyko D. Shoji , and Thomas R. Schibli

*(Invited Paper)*

*Abstract*—The invention of optical frequency combs (OFCs) based on femtosecond (fs) mode-locked lasers has merged laser based spectroscopy with fs-laser technology. OFCs have triggered quantum leaps of advancement in photonics, physics, astronomy, and engineering, while also lending themselves to applications in medical and environmental fields. The key feature of OFCs is their ultrahigh frequency and time resolution. In this review, we introduce the concept behind OFCs and their sources, with a focus on stability and phase-noise performance. We conclude with a discussion of recent progress of a monolithic OFC, which provides ultralow free-running phase noise and an unprecedented frequency stability of 1 part in $10^{19}$ at a 1 s gate time.

*Index Terms*—Phase noise, Laser noise, mode-locked laser, optical frequency comb.

## I. INTRODUCTION

A MODE-LOCKED laser emits a femtosecond pulse train with a stable time interval $\tau_p$ between adjacent pulses and an accumulating phase-shift $\Delta\phi_{CE}$ between the electric field's carrier and the envelope of the pulse as shown in Fig. 1 (top). In the frequency domain, the optical spectrum of the laser exhibits a comb-like structure of discrete longitudinal modes that are evenly spaced by a separation equal to the pulse repetition frequency $f_{rep} = 1/\tau_p$. The carrier envelop offset (CEO) frequency $f_{CEO}$ represents the offset of the first comb line from zero as shown in Fig. 1 (bottom), and can be written as $f_{rep}\Delta\phi_{CE}/2\pi$. Thus, the optical frequency of the $n$th longitudinal modes is given by $\nu_n = f_{CEO} + nf_{rep}$. When $f_{CEO}$ and $f_{rep}$, both of which are in the radio frequency range, are phase locked to an absolute frequency reference (e.g., a cesium clock), every optical frequency in the OFC can be traced back in a phase coherent fashion to the absolute frequency reference that was used to stabilize the OFC [1]. The details of detection and stabilization methods are described in the later section. The OFC is also referred to as an optical ruler.
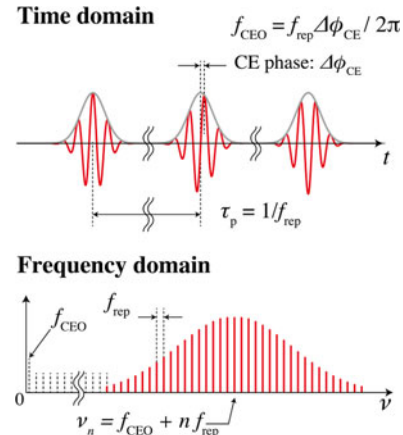


Fig. 1.   Time-frequency correspondence of a mode-locked laser.

Maintaining phase coherence in absolute optical frequency measurements was a challenge in spectroscopic experiments before the emergence of the OFC in the late 1990's. For example, prior to the use of OFCs, measuring a Ca transition in the visible region at $\sim 456$ THz, using a Cs atomic clock at $\sim 9.2$ GHz, required a complex optical-to-microwave link with cascaded phase locked oscillators to maintain phase-coherence [2]. With the invention of the OFC, such coherent links between microwave and optical frequencies can be established relatively easily and carried out on a compact optics table [3], [4]. In particular, OFCs are widely used to measure the frequency of a monochromatic source by measuring the heterodyne beat note between the unknown source and a stabilized OFC. The beat note is again in the radio frequency domain (with a frequency less than $f_{rep}/2$), and it provides information on the phase evolution between the monochromatic laser and the nearest comb tooth of the OFC [1]. Perhaps the most challenging part is determining the integer mode number $n$ of the comb line closest to the unknown source. There are many ingenious applications of OFCs to link optical and microwave signals, such as directly utilizing the light of an OFC to measure the frequencies of absorption features in gas molecules by utilizing a second OFC with a slightly different pulse repetition rate to directly map the optical absorption features to the radio frequency domain. This powerful technique is known as 'dual comb spectroscopy' [5]. Another application involves using OFCs to calibrate the frequency axis of an astronomical spectrometer, which typically rely on optical gratings and arrays of Charge Coupled Devices (CCDs) as detectors; both of which

M. Endo and T. D. Shoji are with the Department of Physics, University of Colorado, Boulder, CO 80309-0390 USA (e-mail: mamoru.endo@colorado.edu; tyko.shoji@colorado.edu).

T. R. Schibli is with JILA, NIST, and the Department of Physics, University of Colorado, Boulder, CO 80309-0440 USA (e-mail: trs@colorado.edu).

exhibit some level of non-uniformity due to manufacturing constraints [6].

OFCs can also be used in the reverse process to transfer the high stability of optical signals into the microwave domain. If the repetition rate of an OFC is stabilized against a low-noise optical reference (e.g., a narrow-linewidth, cavity-stabilized continuous wave (cw)-laser), an ultra-stable microwave can be generated by detecting a harmonic of the pulse repetition rate of the stabilized OFC [7]–[9]. Since the phase noise of the generated microwave is inversely proportional to the square of the frequency ratio, ultra-low phase noise tones can be generated. For example, assuming negligible phase noise from the OFC, the phase noise of a 10 GHz microwave generated from an optical reference of 200 THz would be reduced by $20 \log \frac{10\,\text{GHz}}{200\,\text{THz}} = -86$ dB relative to the phase noise present in the optical reference. However, this dramatic reduction in phase noise is only achieved if the OFC's residual relative phase noise (i.e., after the OFC is stabilized against the optical reference) is significantly below the phase noise of the optical reference. This requires either very large actuator bandwidths to suppress the OFC's intrinsic phase noise, or very low intrinsic noise in the OFC. The best system performance would be achieved with a combination of broad control bandwidths with a low-noise OFC. Such ultra-low noise microwave sources are currently pursued for high-sensitivity Doppler radars [10], with many other potential applications under active development.

In the near future, the current time standards that rely on photonic microwave generation are likely to be replaced by new standards that utilize OFCs to maintain phase-coherence while transferring the signal from optical clocks stabilized to an ionic or neutral atom electronic transition to the radio frequency domain [11]. This is because the requirements and constraints for the OFC performance for optical clocks are rather different from what one would need for photonic microwave generation. The latter requires exquisite phase noise performance (i.e., short-term stability at time-scales ranging from nanoseconds to ∼1 s), whereas clocks typically only require excellent stability for timescales larger than 1 s. Therefore, the metrics for the two fields are slightly different, and microwave performance is generally specified in terms of phase noise (either single as 'sideband phase noise' or the 'spectral density of phase fluctuations,' $L(f)$ or $S(f)$, respectively), whereas the long-term stability of combs is usually specified in terms of an Allan-deviation or the modified Allan-deviation. In Section IV, we will discuss the main sources of phase noise in mode-locked lasers. The required noise performance of the OFC is a crucial factor in determining what type of comb source to use for a given application.

## II. LASER TECHNOLOGIES FOR OFCs

A number of laser technologies have been developed and used for low noise OFC applications. Here we briefly review a few selected examples.

### A. Solid-State Lasers

Early OFCs were based on solid-state lasers, including Ti:sapphire [12]–[19], Cr:LiSAF [20], Cr:forsterate [21],

Yb:KYW [22], Yb:CALGO [23]–[27], and Er:glass [28] lasers, just to name a few. Intracavity dispersion is one of the most important parameters of mode-locked lasers for achieving shorter pulse durations and low noise operation [29], and it is carefully compensated by a prism or grating pair, chirped mirrors or glass plates. Owing to their low-loss cavity configurations (round-trip losses are typically of the order 1–10%), their small net-dispersion, large intracavity pulse energies, and short pulses, solid-state lasers exhibit relatively low intrinsic phase noise, especially at high offset frequencies. A remarkable benefit of Ti:sapphire lasers is their ability to produce octave-spanning spectra directly inside the laser [14], [30]. This removes the requirement of subsequent supercontinuum generation in a non-linear medium, which generally degrades the coherence of the OFC. However, as with most things in laser science, the benefits come in the form of a compromise, and solid-state lasers also have their list of disadvantages. Some of these challenges are related to the mechanical long-term stability and sensitivity to environmental fluctuations. Additionally, the weight and size of the system can be a limitation for certain applications. While solid-state lasers might be competitive cost-wise with other laser technologies, especially since the emergence of cheap, high-power laser diodes [19], [31], the mechanical stability of a free-space laser cavity typically limits the use of such OFCs to optics labs. In a temperature-controlled optics lab however, the latest generation of solid-state laser OFCs have progressed towards stable and reliable OFCs that require minimal user interaction. For instance, Yb or Er-based solid-state lasers pumped by highly-reliable (Telcordia-certified) 980-nm laser diodes and mode-locked by either Kerr-lensing [22], [31]–[33] or by saturable absorber mirrors [25], [26] provide very competitive noise performance in a small physical footprint.

### B. Fiber Lasers

Fiber lasers are good candidates for robust OFCs [29], [34], [35]–[37]. Since almost all of the optical components can be connected by fusion splices or connectors, alignment is unnecessary, which greatly benefits the accessibility and long-term stability of fiber-based OFCs. Stable passive mode-locking is achieved by nonlinear polarization rotation [38]–[43], [44], saturable absorbers (semiconductor saturable absorber mirror: SESAM [45]–[49] and carbon nanotubes [50]) and nonlinear loop mirrors [37], [51], [52]. Rare-earth-doped fibers are readily available, and their emission spectra cover a large range of interesting wavelengths. For instance Er:fiber lasers benefit from the large range of off-the-shelf telecom components, although dispersion management in this wavelength range is somewhat challenging. Yb:fibers is another popular choice due to their ability to cover a particularly useful wavelength range for atomic clocks around 1 $\mu$m (near infrared: NIR) [46], and enable very high power efficiencies due to the small quantum-defect in Yb:glass. For mid-infrared (MIR) applications including molecular spectroscopy, Tm, Ho, and Pr doped or co-doped fiber lasers can be utilized to serve as the oscillators for OFCs [53], [54]. Polarization maintaining gain fibers, photonic crystal

fibers (PCFs) and highly-nonlinear fibers (HNLFs) enable all-fiber OFCs with long-term stability [49], [51], [52]. Such OFCs have been successfully applied to experiments outside of the laboratory [49] and even in space applications [55], [56]. However, this unprecedented robustness comes at the cost of increased intrinsic phase noise. A large part of this phase noise is driven by the large cavity loss (50% or more), large optical non-linearities, limited intracavity pulse energies and relatively large dispersion swings per round-trip. Despite these limitations, Er:fiber OFCs have recently demonstrated absolute frequency instabilities at the level of $3 \times 10^{-18}$ at 1 s gate time [44].

### C. Semiconductor Lasers

A potential candidate for compact, monolithic OFCs is the mode-locked semiconductor laser. At the present time, semiconductor-laser-based OFC designs are based on external (free-space) laser resonators. Currently, the most promising approaches are built on vertical external-cavity surface emitting lasers (VECSELs) with a chirped mirror for dispersion compensation. Such lasers are capable of generating femtosecond pulse trains at repetition rates beyond 1 GHz [57]. Very recently, the CEO frequency of a 1.8 GHz, mode-locked VECSEL has been detected and controlled with an Yb:fiber amplifier and a PCF for supercontinuum generation [58]. The VECSEL chip integrated a SESAM into the cavity, which greatly simplified the design. This kind of semiconductor laser is referred to as a mode-locked integrated external cavity surface emitting laser (MIXSEL) and its repetition rate and pulse duration can reach 100 GHz and 500 fs, respectively [59]. The free-running MIXSEL has been used for dual comb spectroscopy with a narrow-band spectrum [60]. Ongoing work might further improve the cavity loss and dispersion and there seems to be a clear path towards a compact and versatile fs-light source that could serve as an OFC.

The OFCs discussed above are all based on mode-locked lasers. These kind of OFCs are most suitable for applications that require low phase noise. However, another class of OFCs exists that are based on active or passive side-band generation from a cw laser. Such cw laser-based OFCs have the potential to demonstrate high-repetition rates (>10 GHz) and enable OFCs in a robust and compact configuration. Although in this review we focus on mode-locked laser-based OFCs, we briefly introduce two common classes of cw laser-based OFCs: Kerr combs and electro-optic combs. Possible applications include astro-combs [61], high speed telecommunication [62] and low noise microwave generation [63].

### D. Kerr Combs

Launching a cw laser into a small, high-Q optical resonator (microresonator), made from silica, $CaF_2$, $MgO_2$, $Si_3N_4$, or some other suitable optical material, the intracavity power can reach sufficiently high levels to set off broadband cascaded four-wave mixing (FWM). The intracavity FWM process will favor the generation of an equidistant comb whose comb mode spacing coincides with the free spectral range (FSR) of the microresonator or a multiple thereof [64]–[71]. As with most cascaded non-linear processes, the dynamics in such systems are very rich and complex. The small mode-volumes further complicate the dynamics as this typically leads to strong coupling to thermo-refractive effects. As a result, the microresonators offer an attractive way to produce phase coherent OFCs with comb-spacings between 10 GHz and 1 THz, but at the cost of a currently somewhat worse residual phase noise performance. This is a very active field of research with the potential for great developments.

### E. Electro-Optic Combs

Another type of OFC based on cw lasers is the electro-optic (EO) OFC, either based on EO modulators (EOMs) inside a passive enhancement cavity [72], [73] or cascaded EO phase and amplitude modulators [74], [75] that produce a large number of intense side-bands. Such sources are of particular interest for telecommunication applications, that typically require shot-noise limited performance with ~mW-levels of power per comb line at very high-repetition frequencies (typically 50 or 100 GHz). The challenges of this approach include the lack of absolute frequency stability, and the fact that the phase noise of the reference oscillator is multiplied with the side-band number. Therefore, these systems are typically not well suited for applications that require excellent phase noise performance.

## III. OFC STABILIZATION

As outlined in Section I, OFCs have two degrees of freedom, namely $f_{CEO}$ and $f_{rep}$. In this section, we discuss the detection and stabilization of these two frequencies. The basic idea is that if one has an external reference that is more stable than the intrinsic noise or drifts of the OFC, the OFC could be phase-locked to the reference to achieve an OFC with essentially the same stability and noise performance as the external reference it is locked to. Some of the most common techniques and challenges are discussed in the following paragraphs.

### A. Repetition Frequency

The easiest way to detect the repetition frequency is through photodetection of the output pulse train by a fast photodiode. The detected signal contains the repetition frequency and its harmonics, and an error signal can be obtained by mixing one of these harmonics with a local oscillator, such as a Cs-clock disciplined microwave oscillator or hydrogen MASER. While this would provide us with an OFC that could be used as an absolute frequency reference in the optical domain, this method suffers from the fact that the phase noise power spectral density of the reference oscillator is roughly multiplied by the mode number squared ($n^2 \sim 10^8 \ldots 10^{10}$). This leads to a comb with wide optical line widths (e.g., a laser-based OFC tightly locked to a hydrogen MASER typically has a minimum linewidth of ~10 kHz at 200 THz frequencies due to frequency jitter). Ultralow noise OFCs with optical linewidths of the order of 1 Hz or less require an optical reference to stabilize $f_{rep}$. Such an optical reference typically comes in the form of a monochromatic laser, which is phase locked to an ultra-stable optical cavity. One of the longitudinal modes of the OFC and this cavity-stabilized laser

can then be brought to interference to produce a beat signal on a photodetector. The beat signal contains the phase evolution between the comb mode and the optical reference. This beat frequency can then be locked to a microwave reference, or to DC, to avoid a microwave reference altogether.

To perform such a phase lock, the cavity length of the mode-locked laser is tuned by some means (e.g., a piezo electric transducer (PZT) acting on one of the cavity mirrors), which in turn changes $f_{\rm rep}$, or the aforementioned beat note by $n \cdot f_{\rm rep}$. Large but slow drifts of the repetition frequency caused by temperature or air pressure fluctuations can be compensated by temperature control of the laser, e.g., by a Peltier module or a heater, or by a PZT-equipped translation stage. Suppression of fast fluctuations ($>10$ kHz) has been achieved by a variety of methods. One of the most common approaches is mounting a small mirror on a fast PZT to tune the cavity length. The main challenge for this approach is the strong mechanical resonances that can originate from the mechanical recoil of the PZT into the PZT mount. Such resonances can easily limit the achievable locking bandwidth. To suppress such resonances, it is critically important to incorporate appropriate damping and acoustic impedance match techniques in the mount. For example, a thin mirror on a fast PZT mounted on a lead-filled copper mount allows a wide and resonance-free locking bandwidth in excess of 180 kHz [76]. EOMs are another good candidate for fast tuning of $f_{\rm rep}$ as long as the mechanical resonances in the EO crystal are well damped [48], [77]. Both free-space and waveguide-based EOMs have been used for achieving high quality phase stabilization of $f_{\rm rep}$. Generally, the maximum locking bandwidth is ∼1 MHz. For fiber lasers, fibers with a non-zero Verdet constant allow for magneto-optical modulators and can potentially extend the locking bandwidth for stabilizing the cavity length [78].

In general, high bandwidth modulators offer limited dynamic range, and vice versa. Therefore, long-term stabilization of an OFC typically requires a cascade of two or more actuators (often a combination of a slow and a fast actuator as described above).

### B. Carrier Envelope Offset Frequency

The detection of the CEO frequency proves a bit trickier than the detection of the repetition frequency. The main method currently used was first suggested in 1999 [79]. Advances in femtosecond laser technology and the availability of PCFs and HNLFs, have enabled the generation of octave-spanning supercontinua (SC) [80], and enabled the detection of the CEO frequency by what is now known as the $f - 2f$ interferometer [12]. PCFs and HNLF are fibers with tailored dispersion properties (typically near zero dispersion at the seed-wavelength), combined with small cores, confine the optical electric field in a very small cross section. This confinement can be particularly pronounced in air-clad fibers, in which the core is essentially surrounded by air [81]. The combination of the high mode confinement (i.e., high optical intensities), with pulse-preserving dispersive properties, yields significant (i.e., octave spanning) spectral broadening of fs-pulses with just a few 100 pJ pulse energies. A more recent alternative to nonlinear fibers come in form of chip-scale waveguides, such as Si or $Si_3N_4$ waveguides,

which show promise to lower the required input pulse energy even further [24], [82].

After sufficient spectral broadening, a fraction of the long-wavelength light with frequencies around $f_m = f_{\rm CEO} + m f_{\rm rep}$ can be frequency doubled in a second harmonic crystal (usually a periodically polled lithium niobate crystal), which yields a new comb around the frequency $2f_m$. If the spectrum is octave-spanning this frequency may overlap with the short-wavelength range of the comb around a frequency of $f_n = f_{\rm CEO} + n f_{\rm rep}$, for $n = 2m$. An interference between the two frequency components yields the offset frequency $f_{\rm CEO}$ of the comb: $f_n - 2f_m = f_{\rm CEO} + (n - 2m)f_{\rm rep} = f_{\rm CEO}$. Even if the spectrum spans less than an octave, this general approach can still be used by interfering the second and third harmonic components of the short and long wavelength parts of the comb. This approach is sometimes called the $2f - 3f$ interferometer [83].

Since both the $f$ and $2f$ components span a range of optical frequencies, one must take care to maximize the interference between them. This means it is not sufficient to only have good spectral overlap; one would also need to overlap the phase fronts of the electric fields. This requires a good transverse mode-match between the $f$ and $2f$ components, which can be challenging as they originate from components that started out an octave apart from each other. Chromatic aberrations in the optics and the walk-off in the frequency doubling crystal can shift or curve the phase fronts relative to each other. Further, since each spectral component covers a range of frequencies, the resulting pulses must be overlapped in time and the relative optical phase must be within ∼1 rad across each of the two parts to avoid partial destructive interference of the beat note. The former can be avoided by adjusting the relative arm length of the $f - 2f$ interferometer. However, if implemented as a Michelson or a Mach-Zehnder interferometer, one has to be careful about the environmental perturbations that would affect the relative arm length of that interferometer, and hence, would lead to excess noise in the stabilized OFC [45]. A more compact setup that is less prone to environmental noise relies on a common path arrangement. These setups can either be implemented without fine tuning the temporal overlap [77], [84], with an in-line fiber section that can be fusion spliced to the HNLF output [36], or a mechanical method based on a Fabry-Pérot-like etalon, but where the input coupling mirror is a dichroic mirror [46].

In early work, the beat signal strength was usually significantly limited due to the lack of a true octave-spanning spectra. To detect these radio-frequency beat notes, avalanche photodiodes (APD) [12] or photo-multiplier tubes (PMT) [13] were used. However, neither of these detectors offer good linearity, which is important for high dynamic range OFC stabilization. Now, improved nonlinear broadening can be achieved using tapered PCF [85], ultra-HNLF [47] or other approaches [24], [82]. These methods enable sufficiently high optical powers to detect the $f - 2f$ beat note with off-the-shelf PIN photodiodes. PIN photodiodes not only offer much better quantum efficiencies, but also a much higher dynamic range and with very low levels of noise. Ideally, the quantum-limited signal to noise ratio (SNR) of the offset frequency beat note would be solely limited by the shot-noise from the two frequency components (the sum

of the power of the *f* and *2f* components). In reality, excess noise from the nonlinear broadening process and from eventual optical amplification before the broadening process usually further decreases this SNR.

To stabilize the detected CEO frequency, one can essentially employ the same techniques used in $f_{\mathrm{rep}}$ stabilization. However, while it may be tempting to employ a digital phase detector with a built-in divider, as such devices lead to a seemingly more stable lock (i.e., less cycle slips per unit time), it is much more difficult to achieve a coherent OFC when using such devices. The reason is that the residual phase noise with such devices can exceed 1 rad even without encountering cycle slips (typically 1.1·*N*-radians RMS for a division by *N*). This level of residual RMS phase noise in a comb is generally not considered coherent. It is therefore prudent to solely rely on detectors such as analog, doubly balanced mixers (DBM) followed by a low-noise amplifier (LNA) to stabilize the phase of the offset frequency against an external reference, or to DC, by employing the additional methods outlined below.

The CEO frequency, that is CEO phase rate, is related to the ratio of the group and phase velocity inside the laser cavity. This ratio can be controlled by intracavity power modulation via the Kerr effect [34], [86] or group-delay adjustments via cavity alignment [12], [13]. For traditional Ti:sapphire lasers, the pump power is typically modulated by an AOM [16]–[18]. Pump current modulation is often used for LD-pumped mode-locked laser such as Ti:sapphire [19], Yb [22]–[26], [33], [41]–[43], [87] or Er [28], [35]–[38], [44], [49]–[52], [55], [77], [83], [84], [88]–[93] lasers. For these pump power modulation methods, the feedback bandwidth is limited by the stimulated gain lifetime. Typical bandwidths approach several 100 kHz, depending on the gain medium and laser design. Intracavity loss modulators can overcome this limitation. For instance, graphene based loss modulators [54], stimulated emission in the gain [94], and optically pumped SESAMs [27] have been demonstrated.

The above methods often present a considerable amount of cross talk between repetition and CEO frequency changes, which can complicate simultaneous locking of the two degrees of freedom. To overcome this potential limitation an alternative offset locking scheme was devised: in Ti:sapphire [95], Er fiber [48], [96], and $\mathrm{Yb:Y_2O_3}$ ceramic OFCs [33], where extracavity AOMs were used for stabilizing the CEO frequency by applying the appropriate frequency correction to the AOM.

Finally, zero-offset OFCs via difference frequency generation (DFG) have been developed for MIR OFC [97], Yb:fiber [40] or Er:fiber OFCs [91], [93]. The zero offset OFC seed is generated by DFG from two different spectrum regions of SC, and the output is then amplified and the spectrum broadened.

## C. Signal-to-Noise Ratio (SNR)

To get the best residual noise performance in a stabilized OFC, it is important to note that the SNR in the beat notes ($f_{\mathrm{rep}}$ and $f_{\mathrm{CEO}}$) ultimately limit the SNR of the OFC. If the feedback gain at a given frequency exceeds a critical value, such that the in-loop residual noise drops below the noise floor in the beat note, then the feedback loop would actually add incoherent noise to

the OFC, and a lower feedback gain would indeed yield a lower noise comb. In other words, while a beat note with 30 dB in a 300 kHz resolution bandwidth can be locked nearly indefinitely without cycle slips [98], the beat note SNR would limit the phase noise performance of the OFC. This can be of particular interest for photonic microwave generation, where one might want to generate, say a microwave with a 10 GHz carrier and a phase noise floor at −180 dBc/Hz at 10 kHz offset from the carrier. Such a situation would require a beat note SNR of at least 94 dBc/Hz = 180 dBc/Hz–86 dB, or ∼39 dB in 300 kHz resolution bandwidth. (Note that the 86 dB number stems from the estimate presented in the introduction section). Additionally, one will also need to consider all the other noise sources, as the noise power typically adds up incoherently. Such noise sources must include e.g., the SNR in the other degree of freedom, the intrinsic noise of the locking electronics, drifts in the mixer and so on. Summing up the contributions from all the noise terms results in a much more stringent requirement for the SNR (e.g., for the above example, it is likely that ∼50 dB SNR in 300 kHz resolution bandwidth would be required for both beat notes to meet the target performance).

For the aforementioned beat notes, this means that sufficient optical power and a sufficient contrast are required to reach such high SNR values. Recently, SNR of more than 60 dB (100-kHz RBW) has been achieved [99]. To suppress unwanted noise great care should be taken to minimize all other sources of noise, such as shot-noise from comb modes, which do not contribute to the beat note. A simple grating spectrometer or an interference filter placed in front of the photodetector can significantly improve the SNR, or one could employ gated [100] or chirped pulse heterodyne detection [101].

The ultimate SNR is limited by the shot noise of the light at the photodetector, but in practice, optical amplification and SC generation may increase amplitude and phase noise far beyond the shot noise limit. This excess noise is typically larger for combs that are seeded by long pulses or from intrinsically noisy mode-locked lasers. Some details can be found in the references [102], [103]. Dispersion management before the nonlinear broadening is critical as well to maximize the available SNR in the beat notes.

For optical beat notes, one can usually ignore the additive fast noise from other components (not always for direct a lock of $f_{\mathrm{rep}}$ in the microwave domain), such as flicker from PIN diodes and DBMs. Such devices exhibit a flicker noise of approximately −120 dBc/Hz at 1 Hz. The flicker floor decays with $1/f$. Compared to the SNR of the CEO beat signal (∼110 dBc/Hz for state-of-the-art), these values can be negligible. However, for good long-term stability, one will want to select an LNA and a mixer with small temperature-induced bias drifts. Finally, yet importantly, care must be taken to make full use of the SNR going into the DBM, as the output voltage from such devices is typically limited. A well-designed LNA with a few 100 MHz gain-bandwidth product typically has an input voltage noise of a few $\mathrm{nV}/\sqrt{\mathrm{Hz}}$, which includes thermal noise from the resistors [104]. This value should be below the shot noise driven voltage at the DBM output, otherwise the circuit will degrade the SNR.

## IV. NOISE OF MODE-LOCKED LASERS

In the previous section, we discussed the theoretical limits imposed by quantum noise in error signals, and we described how such noise could affect the ultimate noise floor in a stabilized OFC. In that discussion, we mentioned the need for sufficient actuator bandwidths to be able to control all noise that lies above the quantum noise of the error signals. Ideally, the feedback electronics would provide the gain that is matched the OFC's intrinsic noise divided by the quantum noise floor at every offset frequency. This would cause the residual in-loop noise to exactly collapse to the quantum noise floor in the beat notes. However, a subtle but important aspect of this problem lies in the fact that the feedback transfer function must be a causal function. This means that any frequency dependent change in gain will introduce a phase lead or lag. In optics, this effect is well known as the Kramers-Kronig relation. Therefore, the steepest gain slope one can achieve for loop gains larger than unity gain (ignoring the negative sign of the gain for clarity here) without creating an instability is 20 dB per decade. For example, if an actuator has a 100-kHz bandwidth, the gain at 10 kHz is limited to at most 20 dB. Considering this constraint, the residual noise in an OFC might be limited by the limited gain at that frequency and the intrinsic noise of the free-running OFC. Therefore, to achieve the lowest noise stabilized OFC, a combination of high feedback bandwidth, low intrinsic OFC noise and high SNR in the error signal is needed. In this section, we describe some of the most important noise terms that quantify the intrinsic noise of most solid-state laser-based OFDs. The resulting design constraints are then applied to design the monolithic mode-locked laser described in Section V.

In OFCs, the frequency spacing between adjacent comb lines is determined by the repetition rate $f_{\text{rep}}$ of the mode-locked laser. Many applications rely on evenly spaced comb teeth. For example, when generating microwave signals via optical frequency division, any small timing error $\Delta t$ in the temporal spacing between pulses directly introduces phase noise in the microwave carrier through the relation $\Delta\phi \approx 2\pi\Delta t f_{\text{osc}}$, where $f_{\text{osc}}$ is the carrier frequency of the generated microwave signal. It is therefore important to ensure that the timing jitter, or the noise in the repetition rate, is minimized in the mode-locked laser used to generate the frequency comb. Here we provide some brief background on the most significant sources of noise in mode-locked laser systems, following the supplementary material in our previous work with some additions [99]. A more thorough treatment can be found in references [105]–[107]. All phase noise expressions are presented as the single sideband phase noise spectral density $L(f)$.

### A. Timing Jitter Phase Noise PSD Directly Driven by Amplified Spontaneous Emission (ASE)

As the pulse travels through the laser, spontaneous emission from the gain medium introduces noise that can perturb the temporal position of the pulse. For sech$^2$-shaped pulses, the phase noise spectrum contribution from ASE for a 1 Hz bandwidth at an offset frequency $f$ away from the microwave carrier $f_{\text{osc}}$ is

given by

$$L_{\text{ASE}}(f) \approx 0.26\theta g \frac{h\nu}{P}\left(\frac{f_{\text{rep}}f_{\text{osc}}\tau}{f}\right)^2, \qquad (1)$$

where $P$ is the average intracavity pulse power, $\theta$ is the excess noise factor of the laser gain ($\theta \geq 2$ in Er-doped fiber due to the quasi three-level nature of that laser material), $g$ is the round-trip intensity gain (= round-trip cavity loss), $h\nu$ is the photon energy of the laser light, and $\tau$ is the FWHM pulse duration.

### B. Phase Noise PSD Due to Gordon-Haus Jitter

In addition to directly introducing timing noise, ASE can also introduce shifts in the center frequency of the laser's optical spectrum. The shift in center frequency alters the group velocity of the pulse due to dispersion in the cavity. This effect is often the dominant noise source in mode-locked fiber lasers. Assuming a sech$^2$-shaped pulse, the noise contribution from the Gordon-Haus effect can be calculated by

$$L_{\text{GH}}(f) \approx 0.25\theta g \frac{h\nu}{P}\left(\frac{f_{\text{rep}}f_{\text{osc}}\tau}{f}\right)^2$$
$$\times \frac{D^2\Gamma_g^4}{g^2 + 9.26(f/f_{\text{rep}})^2\Gamma_g^4\tau^4}, \qquad (2)$$

where $D$ is the intracavity group delay dispersion and $\Gamma_g$ is the half width at half maximum (HWHM) gain bandwidth or the cavity spectral bandwidth, whichever is smaller.

### C. Phase Noise PSD Due to Self-Steepening

Self-steepening occurs due to the Kerr effect, where light traveling through a medium is subject to an intensity-dependent refractive index. This nonlinearity causes a change in the group velocity, and couples amplitude-to-phase noise. This effect is typically most prominent at low frequencies and is given by

$$L_{\text{ss}}(f) = \frac{1}{2}\left(\frac{f_{\text{rep}}f_{\text{osc}}\varphi_{\text{NL}}}{\pi f\nu}\right)^2 S_{\text{RIN}}(f) \qquad (3)$$

where $\phi_{\text{NL}}$ is the total nonlinear phase shift per round-trip, which is a sum of $\phi_{\text{NL}}$ due to Kerr-nonlinearities and slow saturable absorber response, if present.

### D. Phase Noise Arising From Slow Saturable Absorber Response

For mode-locked lasers with a slow saturable absorber as the phase-locking element, the slow response means that the front of the pulse experiences the greatest amount of absorption. The change in the absorption properties and the pulse shape do not overlap. Consequently, when the absorber responds to a perturbed pulse, the front slope of the pulse generally experiences greater attenuation than the trailing slope, causing the pulse shape to change. This change in the shape of the pulse also shifts the center of the pulse in the time domain. The magnitude of the timing shift depends on the intensity of the pulse, meaning that this process can also convert intensity noise into timing noise. Although often overlooked, the absorber response

can have an appreciable contribution to the timing jitter [108]. The single-sided timing phase noise spectrum arising from the intensity noise is given by [105]:

$$L_{\text{SSA}}(f) = \frac{1}{2} \left( \frac{f_{\text{rep}} f_{\text{osc}}}{f} \frac{\partial \Delta t}{\partial s} s \right)^2 S_{\text{RIN}}(f) \qquad (4)$$

Here, $s = W/E_A$ is the ratio of the pulse energy $W$ over the absorber saturation energy $E_A$. To determine the timing shift $\Delta t$ arising from the slow response of the absorber, we must model the absorber's behavior. For a broad band absorber with negligible coherent effects in the absorber, the timing shift is calculated by

$$\Delta t = \tau_p q_0 h_t(\epsilon, s) s \qquad (5)$$

where $q_0$ is the nonsaturable loss and

$$h_t(\epsilon, s) = \frac{1}{q_0} \int q_s(\epsilon, s) x \, \text{sech}^2(x) \, dx. \qquad (6)$$

Here, $x = t/\tau$ is the time in units of the pulse duration and $\epsilon = \tau/\tau_{\text{abs}}$ is the ratio of the pulse duration over the absorber recovery time. For a $\text{sech}^2$-shaped pulse, the absorber response has the solution.

$$q_s(\epsilon, s) = q_0 \epsilon \int \exp\Big( -\epsilon(x - x')$$
$$- \frac{s}{2} [\tanh(x) - \tanh(x')] \Big) dx' \qquad (7)$$

The absorber response simplifies to an analytic form in the limits of either a very slow ($\epsilon \to 0$), or a very fast absorber ($\epsilon \to \infty$), otherwise $q_s$ must be evaluated numerically.

Using these expressions, the timing shift changes with intensity according to

$$\frac{\partial \Delta t}{\partial s} = \tau \int \frac{\partial q_s}{\partial s} x \, \text{sech}^2(x) \, dx, \qquad (8)$$

where

$$\frac{\partial q_s}{\partial s} = \frac{q_0 \epsilon}{2} \int [\tanh(x') - \tanh(x)] \times \exp\Big( -\epsilon(x - x')$$
$$- \frac{s}{2} [\tanh(x) - \tanh(x')] \Big) dx'. \qquad (9)$$

In light of these expressions, we designed a monolithic mode-locked solid-state laser to strive for the best noise performance in a robust cavity implementation (see next section). The combined effect of these noise sources for the monolithic laser is modeled using measured RIN values and presented in Fig. 2. In this figure, the carrier frequency is assumed to be 1 GHz. The projected phase noise values for different carrier frequencies can be estimated by shifting the traces by $20\log\frac{f_{\text{osc}}}{1\,\text{GHz}}$, except for the shot noise limit (black). For offset frequencies below 10 kHz, the monolithic laser is limited by the noise arising from the slow saturable absorber response. This noise can be eliminated by incorporating a simple RIN eater in the laser system. Moreover, suppressing the RIN can also eliminate $f_{\text{CEO}}$ noise as shown in Fig. 4(c). Above 10 kHz, the Gordon-Haus timing jitter is the dominant source of noise up to an offset frequency
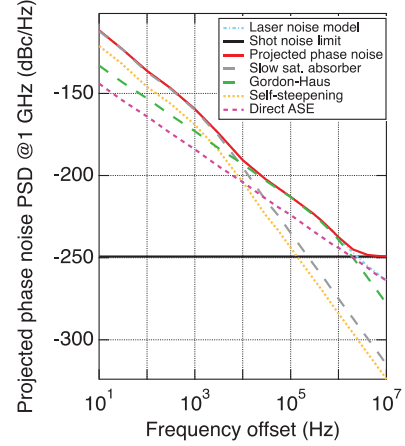


Fig. 2. Projected phase noise PSD of the monolithic laser (red) and the modeled noise contributions from the most significant sources of noise in mode-locked lasers.

of approximately 2 MHz, where the model reaches the quantum limit at $-250$ dBc/Hz due to the limited number of photons inside the laser system.

## V. MONOLITHIC LASER BASED OFC

Considering the noise sources presented above, it becomes clear that to achieve low intrinsic noise, it is important to keep the cavity loss small, the intracavity power high, the pulse duration short, the dispersion and nonlinear phase shift per round-trip as close to zero as possible. It should also be noted that all noise terms scale with the repetition rate to the square, and therefore, lasers with high repetition rates are at a disadvantage. However, to achieve large power per mode from the oscillator, which is required for obtaining a high quantum-limited signal to noise in the beat notes, one will need to compromise between the two noise aspects. For practical reasons, repetition rates between hundreds of MHz to a few GHz are usually desirable for most metrology-related applications.

Another important design constraint is the robustness and long-term reliability of the OFC. Here one might opt for a fiber laser-based OFC due to their maturity and excellent robustness. However, trying to minimize the intrinsic noise from a fiber oscillator is at odds with some of the aforementioned design constraints. While this might be acceptable for most applications, this choice will likely not lead to the lowest noise system. Another consideration is that with very low intrinsic noise, a free-running OFC might suffice, which would greatly simplify the laser system. With all this in mind, we created a monolithic mode-locked solid-state laser that offers the robustness of a well-engineered fiber comb, but with potentially much lower intrinsic noise. This monolithic laser is built from a low-loss $\text{CaF}_2$ cavity, an Er:Yb:glass gain medium, and a SESAM that provides stable, self-starting mode-locking at 1 GHz fundamental repetition rate. The laser emits a femtosecond pulse train with a pulse duration of typically 100–200 fs and a center wavelength of 1556 nm. Thanks to its low round-trip loss and near-zero dispersion configuration, the estimated free-running phase noise are $-160$ dBc/Hz at 1-kHz, $-191$ dBc/Hz at 10-kHz,
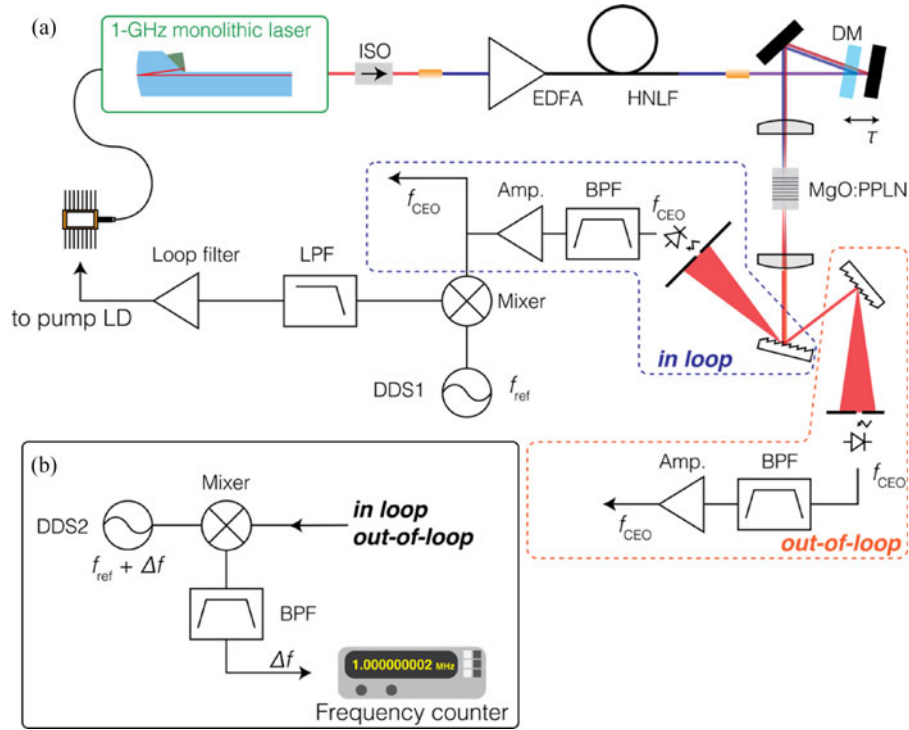
Fig. 3.    (a) Schematic apparatus of out-of-loop $f_{CEO}$ measurement of the monolithic laser based OFC. (b) High-resolution heterodyne measurement technique.

and $-213$ dBc/Hz at 100-kHz offset frequencies at a 1-GHz carrier frequency. Although Kerr-lens mode-locking is ideal for short pulse and low loss cavity configurations, which suppress ASE-related and Gordon-Haus jitters, it requires much larger nonlinear phase shifts per round-trip (typically several hundred mrad, instead of $<9$ mrad for the current monolithic laser design) and potentially higher pump powers. An increase of the nonlinear phase shift would increase the self-steepening effect, and a compromise between these conflicting design goals must be considered.

Some readers may wonder about thermal noise contributions arising from effect such as Brownian motion of the coatings and the $CaF_2$ spacer, or contributions from thermorefractive noise. Such noise usually limits the noise floor of high-finesse cavities and high-Q microresonators [109]. However, in our case, these contributions are all estimated to be far lower than the noise terms discussed in Section IV. For example, Brownian motion noise in the mirror coatings is estimated to contribute at a level of $-136$ dBc/Hz @ 1 Hz offset from a 1 GHz carrier. The spacer noise, excluding thermal expansion, is estimated to contribute at a level of $\sim -160$ dBc/Hz @ 1 Hz offset from a 1 GHz carrier due to the extremely high mechanical Q-factors of $CaF_2$. The thermal noise contributions from the laser glass were neglected in this estimate as these alter the round-trip length by $\sim 1\%$. Thermorefractive noise is believed to be even lower due to the large mode volume.

The monolithic laser was placed inside a copper mount with a Peltier device, and the copper mount was contained within a 3D-printed enclosure (made from polylactic acid). Additionally, the optical breadboard was on a 1-inch urethane sheet and placed within a 1-inch-thick acrylic case. This configuration greatly

suppresses both temperature fluctuations and seismic noise from the environment. In the following experiments where the acquisition time was on the order of ten minutes, this configuration was thermally stable enough to not require active temperature control. For long-term measurement, temperature stabilization might be required due to the relatively high thermal expansion coefficient of $CaF_2$ (18.4 ppm/K, which corresponds to the optical frequency shift of 2 GHz/K). Other materials, e.g., materials with much lower thermal expansion coefficients such as ultra-low expansion (ULE) glass, would help to reduce drifts in the repetition rate. However, the dispersion, loss and birefringence of such materials would spoil the ultra-low noise properties of the monolithic laser. So far, we have not yet found alternative materials to $CaF_2$ for the present operating wavelength range. Further details of the monolithic laser can be found in our previous work [99].

In the following discussion, we highlight a few key features of this monolithic laser source starting with $f_{CEO}$. Fig. 3(a) shows an out-of-loop CEO frequency measurement setup. The output light is guided into an erbium-doped fiber amplifier (EDFA) with four pump diodes and a HNLF for octave-spanning supercontinuum generation. To avoid environmental fluctuations, polarization maintaining fibers are used for these components. After the HNLF, the continuum was guided to a common-pass $f-2f$ interferometer. For CEO frequency detection, the output of the long wavelength part of the spectrum ($\lambda \sim 2.16\,\mu m$) was frequency doubled with a magnesium-doped periodically-poled lithium niobate (MgO:PPLN) crystal, then interfered with the short wavelength part of the spectrum ($\lambda \sim 1.08\,\mu m$). The group delay difference between the two spectral components was compensated by a $\sim 1$ mm long optical delay line using a
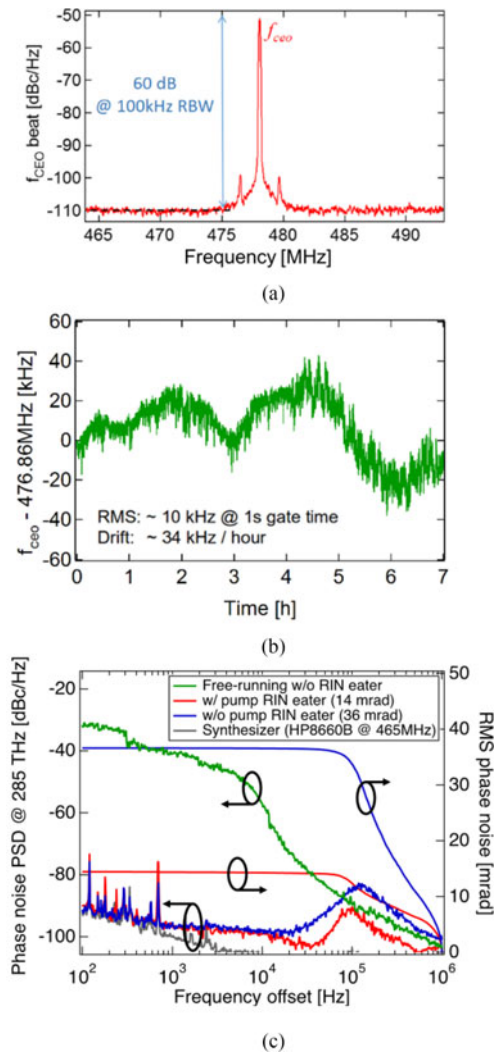
Fig. 4. (a) Free-running $f_{\mathrm{CEO}}$ signal measured with a resolution bandwidth of 100 kHz. (b) Free-running $f_{\mathrm{CEO}}$ fluctuation. (c) Phase noise PSDs (left) and RMS phase noises (right) of stabilized $f_{\mathrm{CEO}}$. Green: free-running, Blue: only with current feedback, Red: with current and RIN feedbacks, Grey: Synthesizer's noise. Reprinted with permission from [99]. Copyright 2016 Optical Society of America. Note that, we added the free-running $f_{\mathrm{CEO}}$ trace in (c) to the original figure in [99].



Fig. 5. Modified Allan deviations of $f_{\mathrm{CEO}}$ at the frequency of 285 THz. Grey: measurement limit, Blue: in loop measurement, Red: out-of-loop measurement.

dichroic mirror as shown in the figure. This configuration has the advantage that almost all optical paths are common-path and the noise from the environment such as air fluctuation can be canceled effectively [46]. To further minimize the effect of the environment, acrylic boxes can be used for the 1-GHz laser and the $f - 2f$ interferometer, though for the data shown in Fig. 4, the $f - 2f$ setup was not enclosed. For the long-term stability measurements, the RF components, such as cables and amplifiers, were covered by urethane foam to stabilize the temperature and to suppress vibrations. The $f_{\mathrm{CEO}}$ signal was detected by an InGaAs PIN photodiode (PD1) after spectral filtering with a diffraction grating and a slit. The detected signal was first bandpass filtered, then amplified by RF amplifiers. A signal-to-noise ratio (SNR) in excess of 60 dB in 100 kHz resolution bandwidth (RBW) was obtained (see Fig. 4(a)). The photocurrent was at least 10 $\mu$A, which corresponds to the shot-noise limited
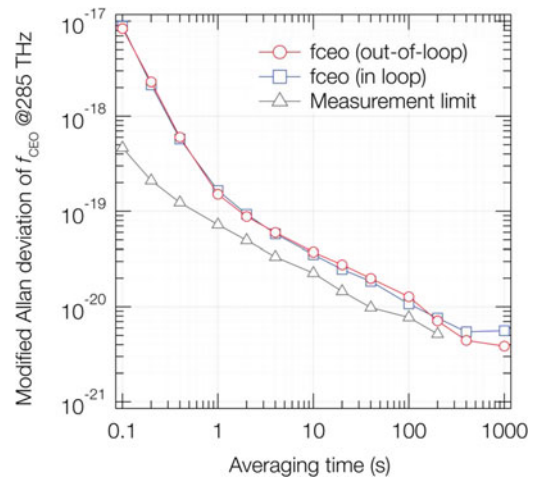
SNR of $\sim$85 dB in 100-kHz RBW. The additional noise was caused by thermal fluctuations in the RF amplifiers. Fig. 4(b) shows the long-term stability of the free-running $f_{\mathrm{CEO}}$ signal (i.e., without any active stabilization). The Allan-deviation for the free-running $f_{\mathrm{CEO}}$ was found to be $\sim 10^{-15}$ at 1 s gate time measured over more than 7 hours. To stabilize this intrinsic noise, the $f_{\mathrm{CEO}}$ beat note was mixed with a reference signal generated by a frequency synthesizer on a DBM and then phase locked with a PID loop filter. After optimization of feedback parameters, the measured phase noise PSD and the RMS phase noise of the $f_{\mathrm{CEO}}$ are shown in Fig. 4(c). The free-running phase noise (green) around the frequency of 100 kHz was limited by the laser RIN. By including a RIN eater, the green trace would be shifted by approximately $-10$ dB. The bump around the frequency range between 1 kHz to 10 kHz is caused by slow drifts of $f_{\mathrm{CEO}}$. Note that the free-running spectrum (green trace) was measured on a different day from the locked spectrum (red trace). The integrated phase noise reaches 14 mrad with the frequency range of 100 Hz to 1 MHz with additional RIN feedback (not shown in Fig. 3(a)). For long-term stability, a modified Allan deviation was also measured with a frequency counter. For this purpose, the $f_{\mathrm{CEO}}$ beat note was mixed with the signal from a direct-digital synthesizer (DDS1) on a DBM and again stabilized by a PID loop filter. The noise floor of this measurement is limited by the frequency counter and the typical limit is $10^{-12}$ for 1 s gate, which corresponds to $7 \times 10^{-19}$ for 1 s gate time in the optical domain ($\sim$285 THz). To improve on this value, we down-converted the $f_{\mathrm{CEO}}$ signal to a lower frequency with a second DDS (DDS2) as shown in Fig. 3(b). For $\Delta f \approx 1$ MHz, the theoretical noise floor becomes $3.5 \times 10^{-21}$ for a 1 s gate time. The down-converted signal was filtered by a bandpass filter (center frequency: 1 MHz, bandwidth: 500 kHz) and then measured by a frequency counter (Keysight, 53230A). The measured Allan deviation is shown in Fig. 5. The grey trace is the detection limit with $7 \times 10^{-20}$ for 1 s gate time, which is one order higher than the theoretical limit of $3.5 \times 10^{-21}$ due to the instability of the DDSs. The blue trace shows the in-loop measurement, in which the same $f_{\mathrm{CEO}}$ signal as the
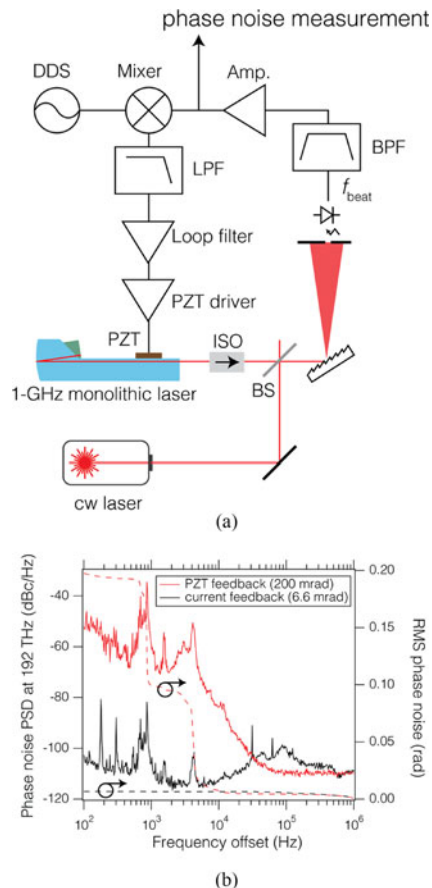
Fig. 6.    (a) Experimental apparatus for $f_{\mathrm{beat}}$ stabilization. BS: beam splitter. (b) The residual phase noise PSD and RMS phase noise of $f_{\mathrm{beat}}$. The large noise peaks between 500 Hz and 1 kHz stem from the cw-laser.

phase locking was used. For a gate time of 1 s, the Allan deviation of $1.8 \times 10^{-19}$ was obtained. For the out-of-loop measurement, the zero-order diffraction light was used. In this case, the measurement is sensitive to environmental fluctuations and a well-isolated box and thermal insulation for all microwave cables and electronics is required. The red trace in Fig. 5 shows the out-of-loop result. The result is well matched to the in-loop result, which means our apparatus was sufficiently well isolated to achieve a $10^{-19}$ level frequency comparison in the optical domain.

For stabilizing the repetition rate, we built a free-running cw laser based on the aforementioned monolithic laser concept, where we replaced the SESAM with a thin air-gap etalon. The beat note between one of the longitudinal modes of the mode-locked monolithic laser and this free-running cw laser was then phase locked as indicated in Fig. 6(a). The beat note was detected by a single InGaAs photodiode (a balanced detector would improve the SNR). A simple grating spectrometer was used do avoid detector saturation from the mode-locked laser. An SNR of 60 dB (100 kHz RBW) after an amplifier (Amp.) was obtained. This value was limited by the RF amplifier noise due to the small optical power from the cw laser (35 $\mu$W). The shot-noise limited SNR would be $\sim$80 dB in 100 kHz resolution bandwidth. The $f_{\mathrm{beat}}$ signal was mixed to the reference signal

from a DDS ($f = 60$ MHz) with a DBM, and then phase locked with a simple PID loop filter. To control the cavity length, a small PZT was placed on the $\mathrm{CaF_2}$ cavity. The PZT was driven by an operational amplifier (Analog Devices, AD8016). To suppress the $\mathrm{CaF_2}$'s mechanical resonances, the cavity was mounted on a lead-filled copper mount. The lead damps the acoustic waves in a similar fashion as described previously in [76]. The residual phase noise PSDs and integrated RMS phase noise are shown in Fig. 6(b). The red traces are for feedback with the PZT (solid: phase noise PSD (left), dashed: RMS phase noise (right)). An RMS phase noise of 200 mrad was obtained, though it should be noted that a large fraction of this noise (e.g., the features between 500 Hz and 1 kHz due to the air-gap etalon) stems from the free-running cw laser. Ultimately, the PZT control still suffers from residual mechanical resonances, and the feedback bandwidth is limited to a few kHz. The black traces show the phase noise PSD and RMS phase noise of the beat note when locked with a much faster current feedback exceeding 100 kHz. This enables the transfer of the free-running noise of the cw laser to the comb. As a result, the residual RMS phase noise drops to an excellent 6.6 mrad.

One interesting observation from the data presented here is that the intrinsic (i.e., free running) linewidth of both the $f_{\mathrm{CEO}}$ and $f_{\mathrm{beat}}$ are of the order of 1 Hz. These values can be found by assuming Lorentzian-like line-shapes at high offset frequencies. This 1 Hz value stands in contrast to typical values on the order of kHz or MHz for the various fiber laser designs in existence. Such low values are only achieved in oscillators that are optimized for very low levels of Gordon-Haus and ASE-induced jitter. Such an optimization was one of the main design goals for these monolithic lasers (see Section IV). The narrow intrinsic linewidths and the robustness of the monolithic laser could accelerate out-of-lab applications, including dual-comb spectroscopy. One could conceive a variation of the current design to create a ring cavity, in which bidirectional mode-locking could be obtained as demonstrated in [110].

## VI. CONCLUSION

With this brief review of state-of-the-art low-noise OFC techniques, we hope to spur future progress toward even lower noise approaches. While the applications for OFCs are too numerous to list, we would like to point out that many of them do not require much beyond what is currently commercially available. However, emerging fields, such as ultra-stable optical clocks, photonic microwave generation, and potentially novel medical diagnostics keep driving the demand of lower noise sources. It is our opinion that the best performance is currently achieved by a combination of active stabilization techniques and low-noise laser designs, but we hope that other approaches might soon be found to drive the field in yet undiscovered and exciting territory.

## REFERENCES

[1] S. A. Diddams, "The evolving optical frequency comb [Invited]," *J. Opt. Soc. Amer. B*, vol. 27, no. 11, pp. B51–B62, 2010.

[2] H. Schnatz, B. Lipphardt, J. Helmcke, F. Riehle, and G. Zinner, "First phase-coherent frequency measurement of visible radiation," *Phys. Rev. Lett.*, vol. 76, no. 1, pp. 18–21, 1996.

[3] T. Udem, J. Reichert, R. Holzwarth, and T. W. Hänsch, "Absolute optical frequency measurement of the cesium d1line with a mode-locked laser," *Phys. Rev. Lett.*, vol. 82, no. 18, pp. 3568–3571, 1999.

[4] S. A. Diddams *et al.*, "Direct link between microwave and optical frequencies with a 300 THz femtosecond laser comb," *Phys. Rev. Lett.*, vol. 84, no. 22, pp. 5102–5105, 2000.

[5] I. Coddington, N. Newbury, and W. Swann, "Dual-comb spectroscopy," *Optica*, vol. 3, no. 4, pp. 414–426, 2016.

[6] T. Wilken *et al.*, "A spectrograph for exoplanet observations calibrated at the centimetre-per-second level," *Nature*, vol. 485, no. 7400, pp. 611–614, 2012.

[7] T. M. Fortier *et al.*, "Generation of ultrastable microwaves via optical frequency division," *Nature Photon.*, vol. 5, pp. 425–429, 2011.

[8] F. N. Baynes *et al.*, "Attosecond timing in optical-to-electrical conversion," *Optica*, vol. 2, no. 2, pp. 141–146, 2015.

[9] X. Xie *et al.*, "Photonic microwave signals with zeptosecond-level absolute timing noise," *Nature Photon.*, vol. 11, no. 1, pp. 44–47, 2017.

[10] P. Ghelfi *et al.*, "A fully photonics-based coherent radar system," *Nature*, vol. 507, pp. 341–345, 2014.

[11] I. Ushijima, "Cryogenic optical lattice clocks," *Nature Photon.*, vol. 9, no. 3, pp. 185–189, 2015.

[12] D. J. Jones *et al.*, "Carrier-envelope phase control of femtosecond mode-locked lasers and direct optical frequency synthesis," *Science*, vol. 288, no. 5466, pp. 635–639, 2000.

[13] A. Apolonski *et al.*, "Controlling the phase evolution of few-cycle light pulses," *Phys. Rev. Lett.*, vol. 85, no. 4, pp. 740–743, 2000.

[14] T. M. Fortier, D. J. Jones, and S. T. Cundiff, "Phase stabilization of an octave-spanning Ti:sapphire laser," *Opt. Lett.*, vol. 28, no. 22, pp. 2198–2200, 2003.

[15] M. S. Kirchner, T. M. Fortier, A. Bartels, and S. A. Diddams, "A low-threshold self-referenced Ti:Sapphire optical frequency comb," *Opt. Express*, vol. 14, no. 20, pp. 9531–9536, 2006.

[16] T. M. Fortier, A. Bartels, and S. A. Diddams, "Octave-spanning Ti:sapphire laser with a repetition rate >1 GHz for optical frequency measurements and comparisons," *Opt. Lett.*, vol. 31, no. 7, pp. 1011–1013, 2006.

[17] A. Bartels, D. Heinecke, and S. A. Diddams, "10-GHz self-referenced optical frequency comb," *Science*, vol. 326, no. 5953, pp. 681–681, 2009.

[18] D. C. Heinecke *et al.*, "Optical frequency stabilization of a 10 GHz Ti:sapphire frequency comb by saturated absorption spectroscopy in r87ubidium," *Phys. Rev. A*, vol. 80, no. 5, 2009, Art. no. 053806.

[19] K. Gürel, V. J. Wittwer, S. Hakobyan, S. Schilt, and T. Südmeyer, "Carrier envelope offset frequency detection and stabilization of a diode-pumped mode-locked Ti:sapphire laser," *Opt. Lett.*, vol. 42, no. 6, pp. 1035–1038, 2017.

[20] R. Holzwarth *et al.*, "White-light frequency comb generation with a diode-pumped Cr:LiSAF laser," *Opt. Lett.*, vol. 26, no. 17, pp. 1376–1378, 2001.

[21] K. Kim *et al.*, "Stabilized frequency comb with a self-referenced femtosecond Cr:forsterite laser," *Opt. Lett.*, vol. 30, no. 8, pp. 932–934, 2005.

[22] S. A. Meyer, J. A. Squier, and S. A. Diddams, "Diode-pumped Yb:KYW femtosecond laser frequency comb with stabilized carrier-envelope offset frequency," *Eur. Phys. J. D*, vol. 48, no. 1, pp. 19–26, 2008.

[23] A. Klenner, S. Schilt, T. Südmeyer, and U. Keller, "Gigahertz frequency comb from a diode-pumped solid-state laser," *Opt. Express*, vol. 22, no. 25, pp. 31008–31019, 2014.

[24] A. S. Mayer *et al.*, "Frequency comb offset detection using supercontinuum generation in silicon nitride waveguides," *Opt. Express*, vol. 23, no. 12, pp. 15440–15451, 2015.

[25] A. Klenner *et al.*, "Gigahertz frequency comb offset stabilization based on supercontinuum generation in silicon nitride waveguides," *Opt. Express*, vol. 24, no. 10, pp. 11043–11053, 2016.

[26] S. Hakobyan *et al.*, "Full stabilization and characterization of an optical frequency comb from a diode-pumped solid-state laser with GHz repetition rate," *Opt. Express*, vol. 25, no. 17, pp. 20437–20453, 2017.

[27] S. Hakobyan *et al.*, "Carrier-envelope offset stabilization of a GHz repetition rate femtosecond laser using opto-optical modulation of a SESAM," *Opt. Lett.*, vol. 42, no. 22, pp. 4651–4654, 2017.

[28] M. C. Stumpf *et al.*, "Self-referencable frequency comb from a 170-fs, 1.5-$\mu$m solid-state laser oscillator," *Appl. Phys. B*, vol. 99, no. 3, pp. 401–408, 2009.

[29] J. Kim and Y. Song, "Ultralow-noise mode-locked fiber lasers and frequency combs: principles, status, and applications," *Adv. Opt. Photon.*, vol. 8, pp. 465–540, 2016.

[30] R. Ell *et al.*, "Generation of 5-fs pulses and octave-spanning spectra directly from a Ti:sapphire laser," *Opt. Lett.*, vol. 26, no. 6, pp. 373–375, 2001.

[31] S. Backus, M. Kirchner, C. Durfee, M. Murnane, and H. Kapteyn, "Direct diode-pumped Kerr Lens 13 fs Ti:sapphire ultrafast oscillator using a single blue laser diode," *Opt. Express*, vol. 25, no. 11, pp. 12469–12477, 2017.

[32] C. G. Durfee *et al.*, "Direct diode-pumped Kerr-lens mode-locked Ti:sapphire laser," *Opt. Express*, vol. 20, no. 13, pp. 13677–13683, 2012.

[33] M. Endo, I. Ito, and Y. Kobayashi, "Direct 15-GHz mode-spacing optical frequency comb with a Kerr-lens mode-locked Yb:Y$_2$O$_3$ ceramic laser," *Opt. Express*, vol. 23, no. 2, pp. 1276–1282, 2015.

[34] N. R. Newbury and W. C. Swann, "Low-noise fiber-laser frequency combs (Invited)," *J. Opt. Soc. Amer. B*, vol. 24, no. 8, pp. 1756–1770, 2007.

[35] F. Adler *et al.*, "Phase-locked two-branch erbium-doped fiber laser system for long-term precision measurements of optical frequencies," *Opt. Express*, vol. 12, no. 24, pp. 5872–5879, 2004.

[36] T. R. Schibli *et al.*, "Frequency metrology with a turnkey all-fiber system," *Opt. Lett.*, vol. 29, no. 21, pp. 2467–2469, 2004.

[37] B. R. Washburn *et al.*, "Phase-locked, erbium-fiber-laser-based frequency comb in the near infrared," *Opt. Lett.*, vol. 29, no. 3, pp. 250–252, 2004.

[38] H. Inaba *et al.*, "Long-term measurement of optical frequencies using a simple, robust and low-noise fiber based frequency comb," *Opt. Express*, vol. 14, no. 12, pp. 5223–5231, 2006.

[39] M. Yan *et al.*, "High-power Yb-fiber comb with feed-forward control of nonlinear-polarization-rotation mode-locking and large-mode-area fiber amplification," *Opt. Lett.*, vol. 37, no. 9, pp. 1511–1513, 2012.

[40] T. Nakamura, I. Ito, and Y. Kobayashi, "Offset-free broadband Yb:fiber optical frequency comb for optical clocks," *Opt. Express*, vol. 23, no. 15, pp. 19376–19381, 2015.

[41] C. Li *et al.*, "1 GHz repetition rate femtosecond Yb:fiber laser for direct generation of carrier-envelope offset frequency," *Appl. Opt.*, vol. 54, no. 28, pp. 8350–8353, 2015.

[42] L. Pang, H. Han, Z. Zhao, W. Liu, and Z. Wei, "Ultra-stability Yb-doped fiber optical frequency comb with $2 \times 10^{-18}$/s stability in-loop," *Opt. Express*, vol. 24, no. 25, pp. 28993–29000, 2016.

[43] B. Xu *et al.*, "Fully stabilized 750-MHz Yb: Fiber frequency comb," *Opt. Express*, vol. 25, no. 10, pp. 11910–11918, 2017.

[44] H. Leopardi *et al.*, "Single-branch Er:fiber frequency comb for precision optical metrology with $10^{-18}$ fractional instability," *Optica*, vol. 4, no. 8, pp. 879–885, 2017.

[45] P. Pal, W. H. Knox, I. Hartl, and M. E. Fermann, "Self referenced Yb-fiber-laser frequency comb using a dispersion micromanaged tapered holey fiber," *Opt. Express*, vol. 15, no. 19, pp. 12161–12166, 2007.

[46] T. R. Schibli *et al.*, "Optical frequency comb with submillihertz linewidth and more than 10 W average power," *Nature Photon.*, vol. 2, no. 6, pp. 355–359, 2008.

[47] I. Hartl *et al.*, "Self-referenced fCEO stabilization of a low noise femtosecond fiber oscillator," in *Proc. Conf. Lasers Electro, Opt. 2008 Conf. Quantum Electron. Laser Sci.*, 2008, Paper CTuC4.

[48] C. Benko *et al.*, "Full phase stabilization of a Yb:fiber femtosecond frequency comb via high-bandwidth transducers," *Opt. Lett.*, vol. 37, no. 12, pp. 2196–2198, 2012.

[49] L. C. Sinclair *et al.*, "Operation of an optically coherent frequency comb outside the metrology lab," *Opt. Express*, vol. 22, no. 6, pp. 6996–7006, 2014.

[50] M. Togashi *et al.*, "Stable operation of all polarization maintaining optical frequency comb based on Er-doped fiber laser with carbon nanotube," in *Proc. Adv. Solid State Lasers*, 2017, Paper JTu2A.47.

[51] E. Baumann *et al.*, "High-performance, vibration-immune, fiber-laser frequency comb," *Opt. Lett.*, vol. 34, no. 5, pp. 638–640, 2009.

[52] N. Kuse, J. Jiang, C. C. Lee, T. R. Schibli, and M. E. Fermann, "All polarization-maintaining Er fiber-based optical frequency combs with nonlinear amplifying loop mirror," *Opt. Express*, vol. 24, no. 3, pp. 3095–3102, 2016.

[53] J. Jiang, C. Mohr, J. Bethge, M. E. Fermann, and I. Hartl, "Fully stabilized, self-referenced thulium fiber frequency comb," in *Proc. Eur. Conf. Lasers Electro-Opt.*, 2011, Paper.

[54] C. C. Lee, S. Suzuki, W. Xie, and T. R. Schibli, "Broadband graphene electro-optic modulators with sub-wavelength thickness," *Opt. Express*, vol. 20, no. 5, pp. 5264–5266, 2012.

[55] J. Lee *et al.*, "Testing of a femtosecond pulse laser in outer space," *Sci. Rep.*, vol. 4, no. 1, 2014, Art. no. 5134.

[56] M. Lezius *et al.*, "Space-borne frequency comb metrology," *Optica*, vol. 3, no. 12, pp. 1381–1387, 2016.

[57] B. W. Tilma *et al.*, "Recent advances in ultrafast semiconductor disk lasers," *Light, Sci. Appl.*, vol. 4, no. 7, pp. e310–e323, 2015.

[58] N. Jornod *et al.*, "Carrier-envelope offset frequency stabilization of a gigahertz semiconductor disk laser," *Optica*, vol. 4, no. 12, pp. 1482–1487, 2017.

[59] C. G. E. Alfieri *et al.*, "Optical efficiency and gain dynamics of mode-locked semiconductor disk lasers," *Opt. Express*, vol. 25, no. 6, pp. 6402–6420, 2017.

[60] S. M. Link, D. J. H. C. Maas, D. Waldburger, and U. Keller, "Dual-comb spectroscopy of water vapor with a free-running semiconductor disk laser," *Science*, vol. 356, no. 6343, pp. 1164–1168, 2017.

[61] X. Yi *et al.*, "Demonstration of a near-IR line-referenced electro-optical laser frequency comb for precision radial velocity measurements in astronomy," *Nature Commun.*, vol. 7, pp. 1–9, 2016, Art. no. 10436.

[62] J. Pfeifle *et al.*, "Coherent terabit communications with microresonator Kerr frequency combs," *Nature Photon.*, vol. 8, no. 5, pp. 375–380, 2014.

[63] W. Liang *et al.*, "High spectral purity Kerr frequency comb radio frequency photonic oscillator," *Nature Commun.*, vol. 6, no. 7957, pp. 1–8, 2015.

[64] I. S. Grudinin, N. Yu, and L. Maleki, "Generation of optical frequency combs with a CaF_2 resonator," *Opt. Lett.*, vol. 34, no. 7, pp. 878–880, 2009.

[65] M. A. Foster *et al.*, "Silicon-based monolithic optical frequency comb source," *Opt. Express*, vol. 19, no. 15, pp. 14233–14239, 2011.

[66] Y. K. Chembo, D. V. Strekalov, and N. Yu, "Spectrum and dynamics of optical frequency combs generated with monolithic whispering gallery mode resonators," *Phys. Rev. Lett.*, vol. 104, no. 10, pp. 103902–103905, 2010.

[67] P. Del'Haye, O. Arcizet, A. Schliesser, R. Holzwarth, and T. J. Kippenberg, "Full stabilization of a microresonator-based optical frequency comb," *Phys. Rev. Lett.*, vol. 101, no. 5, 2008, Art. no. 053903.

[68] V. Brasch *et al.*, "Photonic chip-based optical frequency comb using soliton Cherenkov radiation," *Science*, vol. 351, no. 6271, pp. 357–360, 2016.

[69] T. J. Kippenberg, R. Holzwarth, and S. A. Diddams, "Microresonator-based optical frequency combs," *Science*, vol. 332, no. 6029, pp. 555–559, 2011.

[70] P. Del'Haye *et al.*, "Octave spanning tunable frequency comb from a microresonator," *Phys. Rev. Lett.*, vol. 107, no. 6, 2011, Art. no. 063901.

[71] P. Del'Haye *et al.*, "Optical frequency comb generation from a monolithic microresonator," *Nature*, vol. 450, no. 7173, pp. 1214–1217, 2007.

[72] M. Kourogi, K. Nakagawa, and M. Ohtsu, "Wide-span optical frequency comb generator for accurate optical frequency difference measurement," *IEEE J. Quantum Electron.*, vol. 29, no. 10, pp. 2693–2701, Oct. 1993.

[73] M. Kourogi, T. Enami, and M. Ohtsu, "A monolithic optical frequency comb generator," *IEEE Photon. Technol. Lett.*, vol. 6, no. 2, pp. 214–217, Dec. 2004.

[74] A. Ishizawa *et al.*, "Phase-noise characteristics of a 25-GHz-spaced optical frequency comb based on a phase- and intensity-modulated laser," *Opt. Express*, vol. 21, no. 24, pp. 29186–29194, 2013.

[75] N. Kuse, T. R. Schibli, and M. E. Fermann, "Low noise electro-optic comb generation by fully stabilizing to a mode-locked fiber comb," *Opt. Express*, vol. 24, no. 15, pp. 16884–16893, 2016.

[76] T. C. Briles, D. C. Yost, A. Cingöz, J. Ye, and T. R. Schibli, "Simple piezoelectric-actuated mirror with 180 kHz servo bandwidth," *Opt. Express*, vol. 18, no. 10, pp. 9739–9746, 2010.

[77] K. Iwakuni *et al.*, "Narrow linewidth comb realized with a mode-locked fiber laser using an intra-cavity waveguide electro-optic modulator for high-speed control," *Opt. Express*, vol. 20, no. 13, pp. 13769–13776, 2012.

[78] T. Nakamura, S. Tani, I. Ito, and Y. Kobayashi, "Magneto-optic modulator for high bandwidth cavity length stabilization," *Opt. Express*, vol. 25, no. 5, pp. 4994–5000, 2017.

[79] H. R. Telle *et al.*, "Carrier-envelope offset phase control: A novel concept for absolute optical frequency measurement and ultrashort pulse generation," *Appl. Phys. B*, vol. 69, no. 4, pp. 327–332, 1999.

[80] J. K. Ranka, R. S. Windeler, and A. J. Stentz, "Visible continuum generation in air–silica microstructure optical fibers with anomalous dispersion at 800 nm," *Opt. Lett.*, vol. 25, no. 1, pp. 25–27, 2000.

[81] J. M. Dudley, G. Genty, and S. Coen, "Supercontinuum generation in photonic crystal fiber," *Rev. Modern Phys.*, vol. 78, no. 4, pp. 1135–1184, 2006.

[82] A. R. Johnson *et al.*, "Octave-spanning coherent supercontinuum generation in a silicon nitride waveguide," *Opt. Lett.*, vol. 40, no. 21, pp. 5117–5120, 2015.

[83] K. Hitachi *et al.*, "Frequency stabilization of an Er-doped fiber laser with a collinear 2f-to-3f self-referencing interferometer," *Appl. Phys. Lett.*, vol. 106, no. 23, pp. 231106–231110, 2015.

[84] Y. Kim, S. Kim, Y.-J. Kim, H. Hussein, and S.-W. Kim, "Er-doped fiber frequency comb with mHz relative linewidth," *Opt. Express*, vol. 17, no. 14, pp. 11972–11977, 2009.

[85] T. Jiang *et al.*, "Tapered photonic crystal fiber for simplified Yb:fiber laser frequency comb with low pulse energy and robust f_ceo singals," *Opt. Express*, vol. 22, no. 2, pp. 1835–1841, 2014.

[86] D. R. Walker, T. Udem, C. Gohle, B. Stein, and T. W. Hänsch, "Frequency dependence of the fixed point in a fluctuating frequency comb," *Appl. Phys. B*, vol. 89, no. 4, pp. 535–538, 2007.

[87] Y. Li *et al.*, "Low noise, self-referenced all polarization maintaining Ytterbium fiber laser frequency comb," *Opt. Express*, vol. 25, no. 15, pp. 18017–18023, 2017.

[88] Y. Nakajima *et al.*, "A multi-branch, fiber-based frequency comb with millihertz-level relative linewidths using an intra-cavity electro-optic modulator," *Opt. Express*, vol. 18, no. 2, pp. 1667–1676, 2010.

[89] F. Quinlan *et al.*, "Ultralow phase noise microwave generation with an Er:fiber-based optical frequency divider," *Opt. Lett.*, vol. 36, no. 16, pp. 3260–3262, 2011.

[90] W. C. Swann, E. Baumann, F. R. Giorgetta, and N. R. Newbury, "Microwave generation with low residual phase noise from a femtosecond fiber laser with an intracavity electro-optic modulator," *Opt. Express*, vol. 19, no. 24, pp. 24387–24393, 2011.

[91] D. Fehrenbacher *et al.*, "Free-running performance and full control of a passively phase-stable Er:fiber frequency comb," *Optica*, vol. 2, no. 10, pp. 917–923, 2015.

[92] S. Okubo *et al.*, "Novel phase-locking schemes for the carrier envelope offset frequency of an optical frequency comb," *Appl. Phys. Express*, vol. 8, no. 11, pp. 112402–112406, 2015.

[93] A. Liehl, D. Fehrenbacher, P. Sulzer, A. Leitenstorfer, and D. V. Seletskiy, "Ultrabroadband out-of-loop characterization of the carrier-envelope phase noise of an offset-free Er:fiber frequency comb," *Opt. Lett.*, vol. 42, no. 10, pp. 2050–2053, 2017.

[94] L. Karlen, G. Buchs, E. Portuondo-Campa, and S. Lecomte, "Efficient carrier-envelope offset frequency stabilization through gain modulation via stimulated emission," *Opt. Lett.*, vol. 41, no. 2, pp. 376–379, 2016.

[95] S. Koke *et al.*, "Direct frequency comb synthesis with arbitrary offset and shot-noise-limited phase noise," *Nature Photon.*, vol. 4, no. 7, pp. 462–465, 2010.

[96] K. Nakamura, S. Okubo, M. Schramm, K. Kashiwagi, and H. Inaba, "Offset-free all-fiber frequency comb with an acousto-optic modulator and two f–2f interferometers," *Appl. Phys. Express*, vol. 10, no. 7, pp. 072501–072505, 2017.

[97] T. W. Neely, T. A. Johnson, and S. A. Diddams, "High-power broadband laser source tunable from 30 $\mu$m to 44 $\mu$m based on a femtosecond Yb:fiber oscillator," *Opt. Lett.*, vol. 36, no. 20, pp. 4020–4022, 2011.

[98] L. C. Sinclair *et al.*, "Invited article: A compact optically coherent fiber frequency comb," *Rev. Sci. Instrum.*, vol. 86, no. 8, pp. 081301–081316, 2015.

[99] T. D. Shoji *et al.*, "Ultra-low-noise monolithic mode-locked solid-state laser," *Optica*, vol. 3, no. 9, pp. 995–998, 2016.

[100] J.-D. Deschênes and J. Genest, "Heterodyne beats between a continuous-wave laser and a frequency comb beyond the shot-noise limit of a single comb mode," *Phys. Rev. A*, vol. 87, no. 2, 2013, Art. no. 023802–023807.

[101] J.-D. Deschênes and J. Genest, "Chirped pulse heterodyne for optimal beat note detection between a frequency comb and a continuous wave laser," *Opt. Express*, vol. 23, no. 7, pp. 9295–9312, 2015.

[102] K. L. Corwin *et al.*, "Fundamental noise limitations to supercontinuum generation in microstructure fiber," *Phys. Rev. Lett.*, vol. 90, no. 11, pp. 25–28, 2003.

[103] J. N. Ames, S. Ghosh, R. S. Windeler, A. L. Gaeta, and S. T. Cundiff, "Excess noise generation during spectral broadening in a microstructured fiber," *Appl. Phys. B*, vol. 77, no. 2, pp. 279–284, 2003.

[104] E. Rubiola, "Tutorial on the double balanced mixer," arXiv:physics/0608211, 2006.

[105] R. Paschotta, "Noise of mode-locked lasers (Part II): Timing jitter and other fluctuations," *Appl. Phys. B*, vol. 79, no. 2, pp. 163–173, May 2004.

[106] R. Paschotta, "Noise of mode-locked lasers (Part I): Numerical model," *Appl. Phys. B*, vol. 79, no. 2, pp. 153–162, 2004.

[107] H. A. Haus and A. Mecozzi, "Noise of mode-locked lasers," *IEEE J. Quantum Electron.*, vol. 29, no. 3, pp. 983–996, Mar. 1993.

[108] K. Wu *et al.*, "Towards low timing phase noise operation in fiber lasers mode locked by graphene oxide and carbon nanotubes at 15 $\mu$m," *Opt. Express*, vol. 23, no. 1, pp. 501–511, 2015.

[109] J. Lim *et al.*, "Chasing the thermodynamical noise limit in whispering-gallery-mode resonators for ultrastable laser frequency stabilization," *Nature Commun.*, vol. 8, no. 8, pp. 1–7, 2017.

[110] T. Ideguchi, T. Nakamura, Y. Kobayashi, and K. Goda, "Kerr-lens mode-locked bidirectional dual-comb ring laser for broadband dual-comb spectroscopy," *Optica*, vol. 3, no. 7, pp. 748–753, 2016.

**Mamoru Endo** was born in Kanagawa, Japan, in 1987. He received the B.S, M.S, and Ph.D. degrees in applied physics from the University of Tokyo, Tokyo, Japan, in 2011, 2013, and 2016, respectively. In 2016, he was a Postdoctoral Associate with the Institute for Solid State Physics (ISSP), Kashiwa, Japan, where he worked on high repetition rate optical frequency comb and high-resolution spectroscopy. After that, he was a Research Associate with the Department of Physics, University of Colorado, Boulder, CO, USA, where he currently works on ultralow noise optical frequency combs and microwave generation.

He is a member of the Optical Society of America and the Japan Society of Applied Physics.

**Tyko D. Shoji** was born in Bellevue, WA, USA, in 1990. He received the B.A. degree in liberal arts from Soka University of America, Aliso Viejo, CA, USA, in 2011 and the B.S. degree in physics and mathematics from the Western Washington University, Bellingham, WA, USA, in 2014. He is currently a Graduate Research Assistant with the Department of Physics, University of Colorado, Boulder, CO, USA.

**Thomas R. Schibli** was born in Zürich, Switzerland. He received the Diploma degree in physics from the Swiss Federal Institute of Technology, Zürich, Switzerland, in 1999 and the Ph.D. degree in electrical engineering from the University of Karlsruhe, Karlsruhe, Germany, in 2001.

In 2001, he was a Postdoctoral Associate with the Research Lab of Electronics, Massachusetts Institute of Technology, Cambridge, MA, USA, where he worked on coherent pulse synthesis and ultrashort pulse generation for frequency metrology and time-resolved measurements. In 2003, he was with the National Institute of Advanced Industrial Science and Technology, Tsukuba, Japan, where he worked on compact phase-locked optical frequency combs for frequency and length measurements and frequency synthesis. In 2006, he was with the JILA, Boulder, CO, USA, which is a joint institute between the University of Colorado and the National Institute of Standards and Technology. He is currently a Professor of physics with the University of Colorado, Boulder, CO, USA, and a Fellow Adjunct of JILA.

Dr. Schibli is a member of the Optical Society of America and the American Physical Society.